A SIMPLE 2-DIMENSIONAL MODEL OF SPEED SKATING WHICH MIMICS OBSERVED FORCES AND MOTIONS

D.M. Fintelman[1], O. den Braver[1], and A.L. Schwab[2]

[1]BioMechanical Engineering
[2]Laboratory for Engineering Mechanics
Delft University of Technology
Mekelweg 2, NL-2628 CD Delft, The Netherlands
e-mail: a.l.schwab@tudelft.nl

Keywords: Speed skating, biomechanical model, instrumented speed skate.

Abstract.   *Advice about the optimal coordination pattern for an individual speed skater to reach their optimal performance, could well be addressed by simulation and optimization of a biomechanical model of speed skating. But before getting to this optimization approach one needs a model that matches observed behavior.*

In this paper we present a simple 2-dimensional model of speed skating on the straights which mimics observed kinematic and force data. The primary features of the model are: the skater is modeled as three point masses, only motions in the horizontal plane are considered, air drag forces which are quadratic in the velocity and coulomb type ice friction forces at the skates are included, and idealized contact of the skate on the ice is modeled by a holonomic constraint in the vertical direction and a non-holonomic constraint in the lateral direction. Using the measured leg extension (relative motions of the skates with respect to the upper body) we are able to predict reasonable well the speed skater motions, even if we do not fit for that. The model seems to have the key terms for investigations of speed skating.

1

1   INTRODUCTION

The coordination pattern of speed skating appears to be completely different from all other types of human propulsion. In most patterns of human locomotion, humans generate forces by pushing against the environment in the opposite desired direction of motion. In speed skating humans generate forces by pushing in sideward direction. A skating stroke during speed skating the straights can be divided in three phases: the glide, push-off and reposition phase (Fig. 1). In the push-off phase the skate moves sidewards with respect to the center of mass (COM) of the body till near full leg extension. In the reposition phase the leg is retracted in the direction of the center of mass of the body. During the glide phase the body is supported over one leg that remains at nearly constant height (ankle to hip distance). Double support (both skates on the ice) exists in the first part of the glide phase of one leg and in the second part of push-off phase of the other leg. This coordination pattern results in a sinus-wave like trajectory of the upper body on the ice [2].
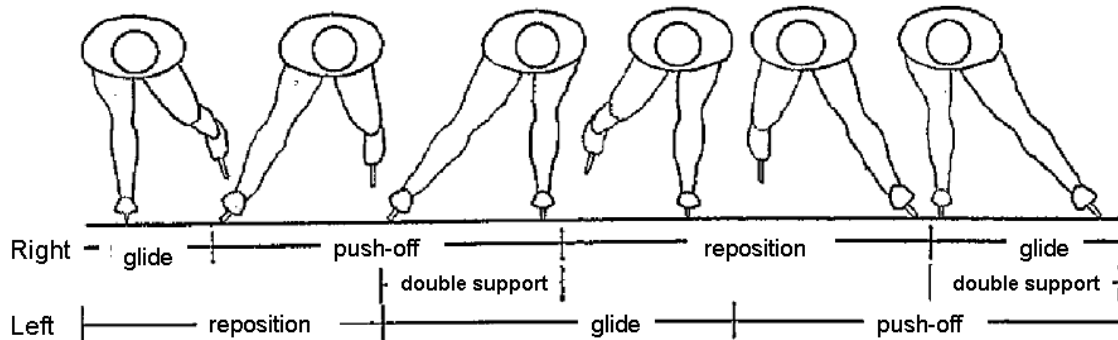
Figure 1: Phases of a stroke: push-off phase, glide phase and reposition phase [1]

Of the many possible coordination patterns (position and orientation of the skates with respect to the upper body), why do skaters use this particular one? What is the optimal coordination pattern for an individual speed skater to reach their optimal performance? How do speed skaters create forward power on ice? Why are speed skaters steering back to their body at the end of the push-off? What is the effect of anthropometric differences on the coordination pattern of a speed skater (like the difference between a tall Dutch skater and a small Japanese skater)? All these questions are highly dependent on the coordination pattern of the speed skater and could well be addressed by simulation and optimization of a biomechanical model of speed skating. But before getting to this optimization approach one needs a model that reasonable matches observed behavior.

Currently, there exist only three speed skating models [11], [7] and [1]. The first models of speed skating were developed by researchers at the VU University Amsterdam [7]. By using power balances of the human and the environment useful information about the posture, athlete physiology and environmental parameters on the performance is provided. Disadvantages of these models are that the validation is difficult and it is impossible to investigate differences in coordination pattern.

A more recent model was developed by Otten [11], in which forward and inverse dynamics are combined. The model is complex and includes up to 19 rigid bodies and 160 muscles. The model is able to simulate skating and can give insight in the forces/moments in the joints. Limitations of the model are that the kinematics in the model are manually tuned and that the

model is not driven and validated with measurements of speed skaters. No information about this model is available in the open literature which makes it hard to review.

The most recent speed skater model is developed by Allinger (University of Calcary)[1]. He developed a simple inverse dynamics model of a speed skater which is driven by individual strokes. The main limitations of the model are that the model is driven by a presumed leg function in time and that the model is not validated with force measurements. Furthermore, the effect of the assumptions on the model (e.g. constant height) are not investigated. On the other hand the model is possibly accurate and very useful for optimization the coordination pattern of speed skating.

Although three biomechanical models exist, none of these models is shown to accurately predict observed forces and motions. Which is partly due to the lack of experimental kinematic data and force data on stroke level.

In this paper, we present a 2-dimensional inverse dynamics model on the straights which has minimal complexity. The model is based on three lumped masses and is validated with observed in-plane (horizontal) kinematics and forces at the skates. In the future, this model can be used to provide individual advice to elite speed skaters about their coordination pattern to reach their optimal performance.

2 METHODS

We measured the 2-dimensional in-plane (horizontal) positions (x, y) of the skates and the upper body, the normal forces and lateral forces at the two skates and lean angle of the skates. We developed a 2-dimensional inverse dynamic model of a skater. The model is driven by the measured leg extensions (relative motions of the skates with respect to the upper body). The upper body motions together with the forces exerted on the ice by the skates are calculated.

A schematic of our 2-dimensional model is shown in Figure 2. The model consists of three point masses: lumped masses at the body and both skates. The total mass of the system is distributed over the bodies by a constant mass distribution coefficient. The motions of the arms are neglected. We do not consider the vertical motion of the upper body, since experiments show that the upper body is at nearly constant height [3]. Air friction and ice friction are taken into account. Idealized contact of the skate on the ice is modeled by a holonomic constraint in the vertical direction and a non-holonomic constraint in the lateral direction.

Values of the mass distribution and air friction are found experimentally. The best agreement between the measurements and model can be achieved if we use accurate values for these parameters. Therefore we constructed an objective function $J_{\min}$ and minimized the error between the measurements and model.

2.1 Analysis of the model

During speed skating modeling, three stages can be distinguished. First, the equations of motion of the speed skater of a single stroke are derived. Secondly, the constraints of all bodies are formulated. Finally all equations are derived in terms of generalized coordinates and solved by numerical integration of these constrained equations of motion.

2.2 Equations of motion

The equations of motion for each separate body (upper body, right skate and left skate) can be derived in x and y direction. Friction forces (air and ice friction) as well as the constraint forces are acting on the bodies. All constraints acting on the bodies will be explained in the
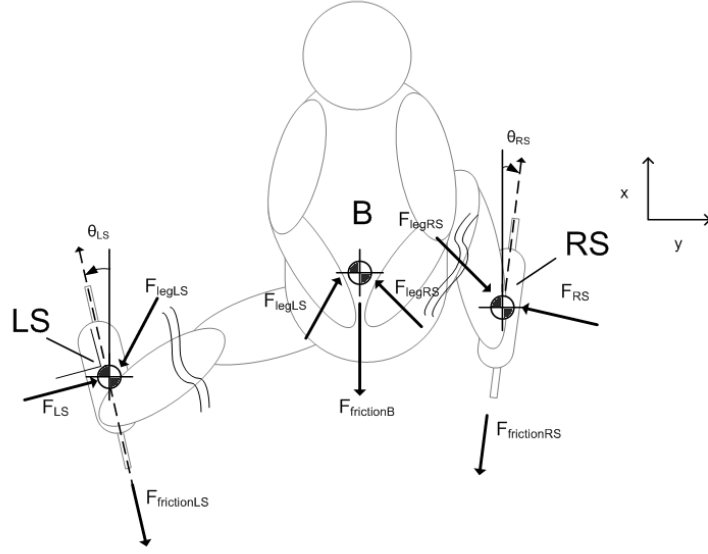
Figure 2: Free body diagrams of the three point mass model (horizontal plane, top view). The masses are located at the COM of the body and at the COM of the skates. F_{ls} and F_{rs} are perpendicular with the skate blades, θ_{ls} and θ_{rs} are the steer angles of the skates with respect to the x-axis. The x- and y-axis are the inertial reference frame fixed to the ice rink

next paragraph. The equations of motions for all bodies are,

$$
\begin{aligned}
m\ddot{x}_i &= -F_{frictionX_i} + F_{constraintsX_i} \\
m\ddot{y}_i &= -F_{frictionY_i,} + F_{constraintsY_i} \qquad i = B, LS, RS
\end{aligned}
\tag{1}
$$

where $F_{frictionX_i}$ is the component of the friction force in x direction and $F_{frictionY_i}$ the component of the friction force in y direction. $F_{constraintsX}$ are the constraint forces in x direction and $F_{constraintsY}$ the constraint forces in y direction.

2.3 Constraints

The first set of constraints are the leg extension constraints, they connect the skates to the upper body. The positions of the skates are prescribed by the position of the upper body and the leg extension coordinates. The second set of constraints are at the skates. A holonomic constraint is applied in the vertical direction which establish that the skate is on the ice and a non-holonomic constraint in the lateral direction of the skate to express that there is no lateral slip of the skate on the ice.

2.4 Generalized coordinates

We like to express the coordination of the motion of the skater in terms of the leg extensions. Therefore the configuration of the skater is expressed by the motion of the upper body and the leg extensions (relative motions of the skates with respect to the upper body, see Fig. 3) and expressed by the generalized coordinates,

$$
\mathbf{q} = (xb, yb, u_{LS}, v_{LS}, \theta_{LS}, u_{RS}, v_{RS}, \theta_{RS})^T,
\tag{2}
$$

in which θ_{LS} and θ_{RS} are the steer angles of the skates with respect to the x-axis. These steer angles, which are prescribed coordinates, are only needed to apply the non-holonomic skate

constraints. The equations of motion will be written in terms of the generalized coordinates. Detailed information on the transformation of the equations of motions in terms of the generalized coordinates can be found in Appendix A, H, and I.
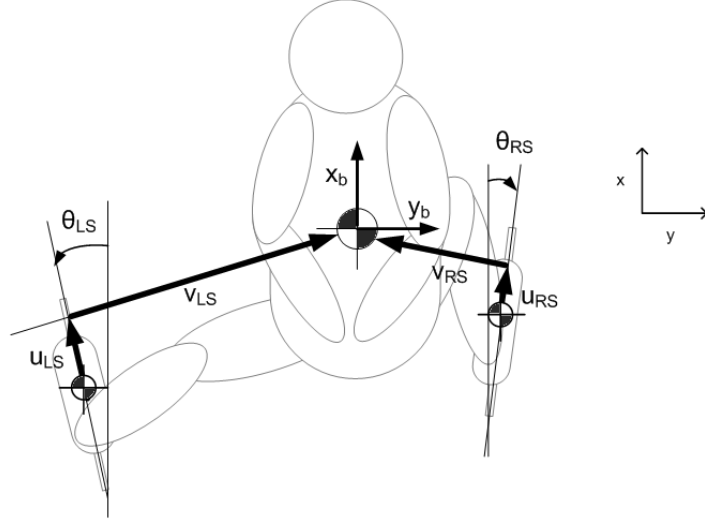
Figure 3: Definition of generalized coordinates

2.4.1 Leg extension constraints

The position of the right and left skate can be expressed as function of the generalized coordinates. The left skate leg extension constraints are,

$$c_1 = x_{LS} - x_B + \cos\left(\theta_{LS}\right) u_{LS} + \sin\left(\theta_{LS}\right) v_{LS} = 0, \tag{3}$$

$$c_2 = y_{LS} - y_B - \sin\left(\theta_{LS}\right) u_{LS} + \cos\left(\theta_{LS}\right) v_{LS} = 0. \tag{4}$$

And the right skate leg extension constraints are,

$$c_3 = x_{RS} - x_B + \cos\left(\theta_{RS}\right) u_{RS} + \sin\left(\theta_{RS}\right) v_{RS} = 0, \tag{5}$$

$$c_4 = -y_{RS} + y_B - \sin\left(\theta_{RS}\right) u_{RS} + \cos\left(\theta_{RS}\right) v_{RS} = 0. \tag{6}$$

2.4.2 Skate constraints

When the skate is on the ice we assume no lateral slip between the ice and skate, that is the lateral velocity of the skate is zero. This can be expressed by a non-holonomic constraint which are for the left and right skate respectively,

$$c_5 = -\sin\left(\theta_{LS}\right) \dot{x}_{LS} - \cos\left(\theta_{LS}\right) \dot{y}_{LS} = 0, \tag{7}$$

$$c_6 = -\sin\left(\theta_{RS}\right) \dot{x}_{RS} + \cos\left(\theta_{RS}\right) \dot{y}_{RS} = 0. \tag{8}$$

Since we do not consider vertical motions no constraints in the vertical direction are needed. Contact or no contact is described by on/off switching of the non-holonomic constraint.

2.5 Mass distribution

The number of bodies in the model is based on an investigation of the shift in position of the center of mass on a complete anthropometric model of a speed skater during the gliding and the push-off phase of a stroke. A minimum of three bodies was shown to be necessary for describing the shift of the center of mass [5].
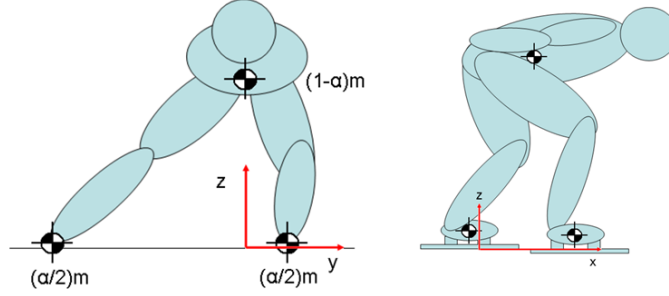
Figure 4: Positions of the COM of the bodies during the push-off together with the mass distribution.

The total mass m of the skater is now distributed over the three point masses (body, left skate, right skate) by using a mass distribution coefficient α (Fig. 4). The distribution of the masses are given by $m_B = (1 - \alpha)m$, $m_{LS} = (\alpha/2)m$, and $m_{RS} = (\alpha/2)m$.

2.6 Friction forces

The total friction forces can be roughly divided in 80% air friction and 20% ice friction [8]. The ice friction in the model, following de Koning [9], is described by Coulomb's friction law,

$$F_{\text{ice}} = \mu F_N \tag{9}$$

where μ is the friction coefficient and F_N the normal force of the skate on the ice. Here we assume that the height of the skater is constant and that there is no double stance phase. Therefore, the ice friction can be written as $F_{\text{ice}} = \mu m g$ in which m the mass of the skater and g the earth gravity. The air friction can be described by,

$$F_{\text{air}} = \frac{1}{2}AC_d\rho v^2 = k_1 v^2 \tag{10}$$

where Cd represents the drag coefficient, A the frontal projected area of the skater, ρ the air density and v the velocity of the air with respect to the skater. The air drag forces at each individual mass are calculated by multiplying the mass distribution coefficient of that mass by the total air drag. The drag coefficient k_1 can only be estimated experimentally. With an experimental method (see Appendix E) both the drag coefficients μ and k_1 for every individual subject are estimated.

2.7 Model summary

The equations of motion together with the constraint equations are completely defined by the state of skater. Combining the equations of motion for the individual masses (1) and including of the constraint forces and the constraints (3 - 6) on the acceleration level results in the constraint

6

equations of motion for the system, $\mathbf{Au} = \mathbf{b}$, with

$$
\mathbf{A} = \begin{bmatrix}
m(1-\alpha) & 0 & 0 & 0 & 0 & 0 & -1 & 0 & -1 & 0 \\
0 & m(1-\alpha) & 0 & 0 & 0 & 0 & 0 & -1 & 0 & 1 \\
0 & 0 & \frac{\alpha}{2}m & 0 & 0 & 0 & 1 & 0 & 0 & 0 \\
0 & 0 & 0 & \frac{\alpha}{2}m & 0 & 0 & 0 & 1 & 0 & 0 \\
0 & 0 & 0 & 0 & \frac{\alpha}{2}m & 0 & 0 & 0 & 1 & 0 \\
0 & 0 & 0 & 0 & 0 & \frac{\alpha}{2}m & 0 & 0 & 0 & -1 \\
-1 & 0 & 1 & 0 & 0 & 0 & 0 & 0 & 0 & 0 \\
0 & -1 & 0 & 1 & 0 & 0 & 0 & 0 & 0 & 0 \\
-1 & 0 & 0 & 0 & 1 & 0 & 0 & 0 & 0 & 0 \\
0 & 1 & 0 & 0 & 0 & -1 & 0 & 0 & 0 & 0
\end{bmatrix} \tag{11}
$$

$$
\mathbf{u} = \begin{bmatrix} \ddot{x}_B & \ddot{y}_B & \ddot{x}_{LS} & \ddot{y}_{LS} & \ddot{x}_{RS} & \ddot{y}_{RS} & \lambda_1 & \lambda_2 & \lambda_3 & \lambda_4 \end{bmatrix}^T \tag{12}
$$

$$
\mathbf{b} = \begin{bmatrix} -F_{XfrictionB} & -F_{YfrictionB} & -F_{XfrictionLS} & -F_{YfrictionLS} & -F_{XfrictionRS} \\ -F_{YfrictionRS} & hc_1 & hc_2 & hc_3 & hc_4 \end{bmatrix}^T \tag{13}
$$

Where $hc_1 \cdots hc_4$ are the convective acceleration terms of the constraints (Appendix I) and $\lambda_1 \cdots \lambda_4$ are the constraint forces (Lagrange multipliers). Here λ_1 and λ_2 are the constraint forces in the left leg, and λ_3 and λ_4 the constraint forces in the right leg. The non-holonomic skate constraints are not yet included in this system.

The model exists of 3 bodies with each 2 degrees of freedom, thus the unconstrained system has 6 degrees of freedom. However, there are 4 coordination constraints and 1 constraint of the skate on the ice (no double stance); therefore 1 degree of freedom remains. If there is a double stance phase then both skates are on the ice and no degree freedom is left. Therefore in our idealization, the model will alternatively switch between the right skate en left skate constraint.

We rewrite the equations of motion (11 - 13) (still without the non-holonomic skate constraints) in terms of the generalized coordinates (2), where the prescribed coordinates (leg extension coordinates $(u_{LS}, v_{LS}, \theta_{LS}, u_{RS}, v_{RS}, \theta_{RS})$) are pushed to the right-hand side (Appendix A). Next, the constraint of the skate on the ice (left or right) is added to the equations. Finally the reduced constrained equations of motion are given by, for when the left skate is on the ice,

$$
\begin{bmatrix} m & 0 & -s_{LS} \\ 0 & m & -c_{LS} \\ -s_{LS} & -c_{LS} & 0 \end{bmatrix} \begin{bmatrix} \ddot{x}_B \\ \ddot{y}_B \\ \lambda_5 \end{bmatrix} = \begin{bmatrix} \mathbf{T}_{,\mathbf{q}}^T(\mathbf{f} - \mathbf{Mh}) \\ hc_5 \end{bmatrix}, \tag{14}
$$

and for when the right skate is on the ice,

$$
\begin{bmatrix} m & 0 & -s_{RS} \\ 0 & m & c_{RS} \\ -s_{RS} & c_{RS} & 0 \end{bmatrix} \begin{bmatrix} \ddot{x}_B \\ \ddot{y}_B \\ \lambda_6 \end{bmatrix} = \begin{bmatrix} \mathbf{T}_{,\mathbf{q}}^T(\mathbf{f} - \mathbf{Mh}) \\ hc_6 \end{bmatrix}, \tag{15}
$$

where λ_5 and λ_6 are the lateral constraint forces on the skate and hc_5 and hc_6 are the convective acceleration terms of the skate constraints, the latter are presented in Appendix I. Clearly both systems have one degree of freedom left, one can think of it as being the forward motion.

Table 1: Parameter values for the four riders.

Variable	Description	Value
m	Mass skater	66, 80, 77, 84 [kg]
α	Mass distribution	0.604, 0.682, 0.607, 0.686 [-]
k_1	Drag coefficient	0.160, 0.153, 0.112, 0.299 [N/(m/s)^2]
g	Gravity	9.81 [m/s^2]

2.8 Model constants

Listed in Table 1 are the values of the model parameters used in the simulations. The total mass of the skater is a measured quantity. The other parameters are found by an optimization process as described in Appendix C.

3 MODEL ANALYSIS

3.1 Parametrization of the coordination body functions

To determine the velocities and the accelerations of the bodies, all measured positions have to be numerical differentiated. To get rid of model errors due to differential and filtering errors (spikes), all positions are first parameterized. The required parametrization functions have to be twice differentiable. The combination of a linear and periodic functions satisfies this requirement. The used parametrization function is, 16.

$$f = c_0 + c_1 t + \sum_{k=1}^{5} a_k \sin\left(2k\pi\frac{t}{T}\right) + b_k \cos\left(2k\pi\frac{t}{T}\right) \tag{16}$$

The fit is not accurate at the beginning and end of the stroke, which results in a mismatch of the initial conditions on the velocities and accelerations. Therefore the coordinates are fit at a longer time period and be cut off afterwards. We tried also other parametrization functions, like polynomial and cubic splines. The differentials of polynomial functions became unstable with increasing order, while piecewise cubic splines has no filtering which results in high frequent components in the positions. The measured positions of the body, left and right skate in x and y direction of a single stroke are parameterized according to (16) and by differentiating the equations of the fitted function the velocities and acceleration are calculated.

3.2 Integration of the differential equations

The differential algebraic equations (14,15) describing the motion of the system can not be solved analytically. Therefore, the equations will be numerically integrated, using the classic Runge-Kutta 4th order method (RK4). The stepsize h is taken constant during the whole simulation, and chosen identical to the sample time of the measurements $T_s = 1/100$ [sec]. After each numerical integration step the constraints are fulfilled by a projection method (Appendix B).

3.3 Data collection

The data collection of the skater includes the 2-dimensional in-plane positions (x, y) of the two skates and the upper body, the normal and lateral forces at the two skates and lean angle of the skates. The global positions are measured by a radio frequency based so-called local position

8

measurement system (LPM) from Inmotio[1]. This system is installed at the Thialf speed skate rink in Heerenveen, The Netherlands. The LPM system has been used for analysis of soccer matches, and can handle up to 22 active transponders at 1000/22 Hz. The transponders are approximately placed at the positions of the point masses.

We have developed two instrumented clap skates to measure the normal and lateral forces (N_i, L_i) at the blades of the skates, see Figure 5). To be able to compare these with the model output, which are the global lateral forces F_{Tls} and F_{Trs}, the lean angles of the skates, ϕ_i, must be measured.
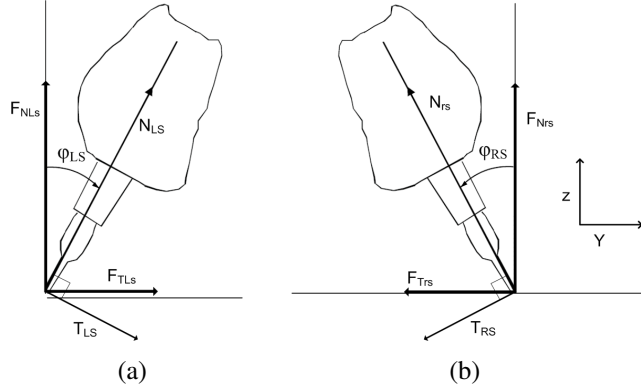
Figure 5: Forces in local reference frame (N_{ls}, T_{ls}, N_{rs}, T_{rs}) and global reference frame (F_{Nls}, F_{Tls}, F_{Nrs}, F_{Trs}): a) left skate b) right skate

A DAQ of National instruments [2] is used for data acquisition of the forces. All the force and orientation data is collected on a mini laptop which is carried by the skater in a backpack. The different measurement systems are synchronized by means of images from a high speed camera. See appendix D for detailed description of the synchronization method.

Data sets of four trained speed skaters are used to validate the model. The data collection is performed with a standard measurement protocol which includes: skating two laps at an estimated 80% of maximal performance level. The tests are repeated at least three times.

3.4 Fitting the model to the observed data

The model is validated by showing how closely it can simulate the observed forces and motions. Quantification of the model errors are analyzed similar to that of McLean [10]. The measured data has different scales and units and therefore we constructed a measurement of error, $J_{\min}$, between the model and the measured data which includes the error of the upper body position, velocities and local normal forces (N_{ls} and N_{rs}). The measurement of error is dimensionless, reasonably scaled and independent of the number of time samples. See Appendix C for a detailed description of the measurement error function $J_{\min}$.

4 RESULTS

Plots of the measured and simulated forces and motions (output of model) as a function of time for a sequencing left and right stroke are shown in Figure 7 (The parameters are according

---

[1]http://www.inmotio.nl, Hettenheuvelweg 8, 1101 BN Amsterdam Zuidoost, The Netherlands.
[2]www.ni.com

to the first rider from Table 1). The corresponding measured and parameterized leg extensions (input of model) of the left and right leg are shown in respectively Figure 6(a) and Figure 6(b). At the beginning of the left stroke ($t = 0$) the skate is placed in front of the upper body, resulting in a negative u_{ls}. During the stroke the skate is moving sidewards and backwards, u_{ls} and v_{ls} increase. At the end the stroke the skate is retracting to the upper body, u_{ls} and v_{ls} decrease. At the beginning of the right stroke ($t = 1.25$), the skate is again moving sidewards, v_{rs} increase. However the motion pattern of the u_{rs} is somewhat different in comparison with u_{ls}. The u_{ls} remains approximately constant during the stroke, which results in a different output motion of the upper body in y direction.
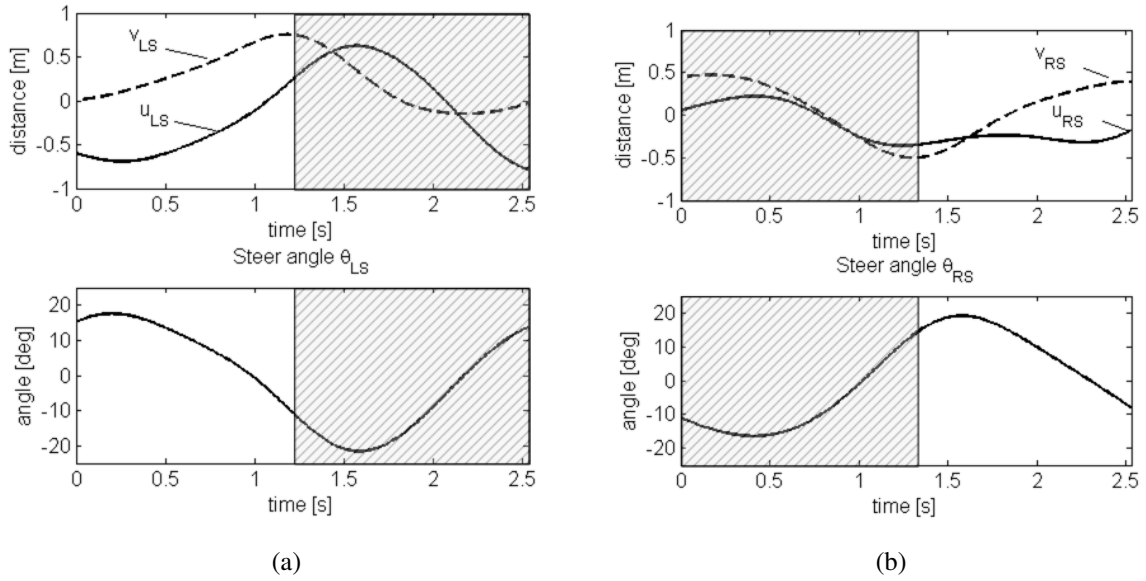
Figure 6: Measured and parameterized leg extension coordinates u_i, v_i and θ_i as a function of time for a sequencing left and right stroke for rider 1 from Table 1. Gray filled area mean that the skate is not active. a) left skate, b) right skate

The skater has an average forward speed of $\approx$ 32 km/h. The upper body describes a sine-wave like trajectory with respect to the ice during speed skating the straights (Fig. 7(a) y_b), which has also been observed by de Boer [2]. The velocity pattern sidewards, $\dot{y}_b$, are alike for left and right stroke. However, the forward acceleration/deceleration pattern differ per stroke. This was observed for every rider.

The local normal forces N_{LS} and N_{RS} of the active skate are shown in Figure 7(b), where the height of the body is assumed constant. At the large force drop in the measured force date a switch is made in the model from the left skate to the right skate. Note that the sum of the measured left and right force corresponds well to the calculated value. At the beginning of the stroke the normal force is rising above the body weight of the skater. Then a small force drop appears and at the end of stroke the normal forces rises again well above the body weight. The maximal normal force during push-off is approximately 150% of the body weight.

Agreement exists between the measured and simulated positions and velocities. The largest error is in the force data, which mainly appears at the beginning and end of the stroke.

For all skaters the net error $J_{\min}$ (24) of all straight left strokes is calculated. This net error is divided by the number of optimization parameters being the upper body positions, upper body velocities and the local normal forces and presented in Table 2.

10
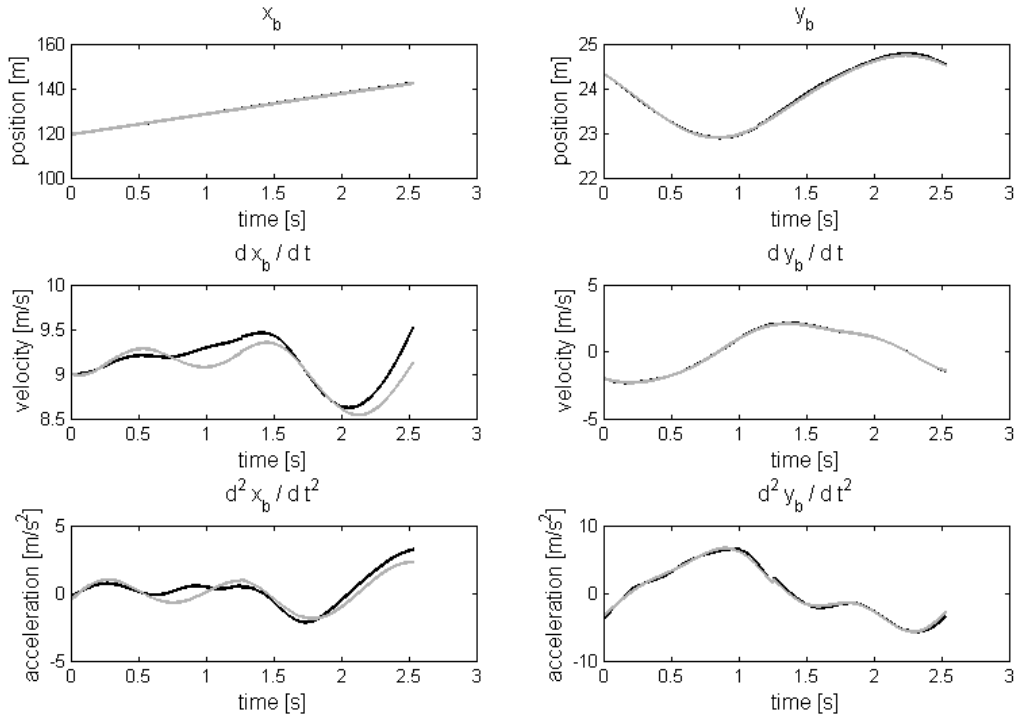
(a)
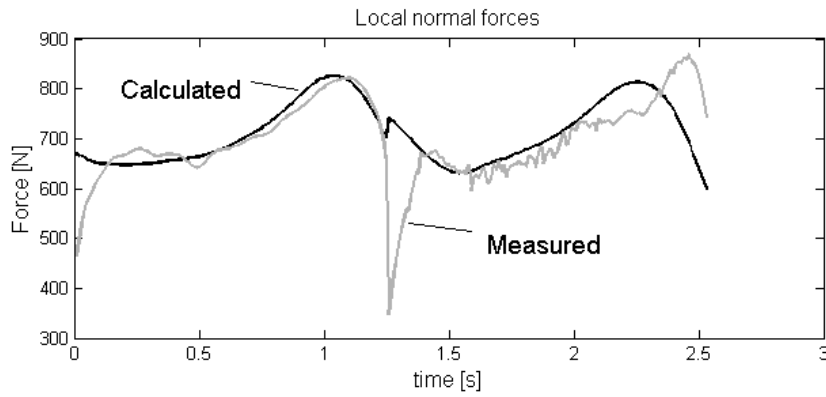
(b)

Figure 7: Simulated (black lines) and measured (gray lines) upper body positions, velocities, accelerations and local normal forces on the skates (N_i), as a function of time for a sequencing left and right stroke, for rider 1 ($m = 66$ kg) from Table 1

Table 2: Net error $J_{\min}$ per subject (average of all left straight strokes of all tests) divided by the number of optimization parameters

Skater	$J_{\min}$
1	0.0013
2	0.0015
3	0.0022
4	0.0013

11

Averages of the magnitudes of the residuals are calculated similar to that of Cabrera [4] by $R_j = \sum\limits_{i=1}^{N} |\tilde{y}_{ij} - y_{ij}|/N$. In which N the number of collected data points, y_i the measured value of the variable and $\tilde{y}_i$ the simulated value of the variable from the model. For all variables j the R_j is shown in Table 3. The residuals of the upper body are less than 0.10 m for the forward position, 0.031 m sidewards, 0.20 m/s in the forward velocity, 0.06 m/s sidewards, and 53 N for the local normal forces in the skate.

Table 3: Table of the residuals between measured and simulated values of the variables. Body position in x direction [m], body position in y direction [m], body velocity in x direction [m/s], body velocity in y direction [m/s], body acceleration in x direction [m/s^2], body acceleration in y direction [m/s^2], local normal forces [N]

Skater	R_{xb}	R_{yb}	$R_{\dot{x}b}$	$R_{\dot{y}b}$	$R_{\ddot{x}b}$	$R_{\ddot{y}b}$	R_{Nl}
1	0.0795	0.0165	0.1769	0.0464	0.5880	0.3836	22.01
2	0.0817	0.0245	0.1659	0.0491	0.5952	0.3379	34.30
3	0.1048	0.0314	0.2071	0.0626	1.0276	0.3244	53.91
4	0.0782	0.0186	0.1737	0.0401	0.8315	0.2380	26.45

5 DISCUSSION

5.1 Model error

All position residuals are within the accuracy of the position measurement system (≈ 0.15 m). The accuracy of the LPM can be increased if two transponders, instead of one transponder are positioned at the skates and the upper body. The forward velocities $\dot{x}_B$ are less accurate than the sideward velocities $\dot{y}_B$, which is reasonable due to the fact that the forces are mainly in sideward direction instead of forward. Orientation errors have therefore more influence on the $\dot{x}_B$ as on the $\dot{y}_B$.

No total agreement exists between the measured forces and the forces calculated in the model, generally at the beginning and at the end of the stroke. There is no normal force drop in the calculated data which is a result of the simplification that there is no double stance phase, but the sum of the measured left and right force do correspond well with the calculated one. Conversion from global to local forces resulted in a force error, caused by the accuracy of the lean angle sensors. The accuracy of these sensors are < 2 deg root mean square, resulting in a local normal force error between $\approx 20/-20N$. Besides conversion errors, crosstalk exists of $\approx 3\%$ of the lateral forces to the normal forces (max. $-9/9$ N). The maximal error due to inaccuracy of the measurement equipment is then approximately 29 N.

The net error $J_{\min}$ of all measurements are in the same magnitude, which shows that the model is valid for all subjects.

5.2 How does the fit depends on mechanical constants

The sensitivity of the mechanical constants is obtained by minimizing the net error $J_{\min}$ (24). This net error is calculated by letting the upper body motions variable while fixing all other parameters to their optimal fit value, except for the wanted minimization parameter (mass distribution α, air friction coefficient k_1 or mass of the skater m). In Figure 8 the normalized net error $J_{\min}$ are plotted as function of the minimization parameters. The minimal values in the figures corresponds to the values of the parameters at the optimal fit.

The mass is the most sensitive mechanical parameter, however this parameter is measured accurately and therefore of no concern here. The value of the mass distribution α as well as the friction coefficient k_1 are more uncertain. The figure shows clearly that the fit depends little on these mechanical constant.
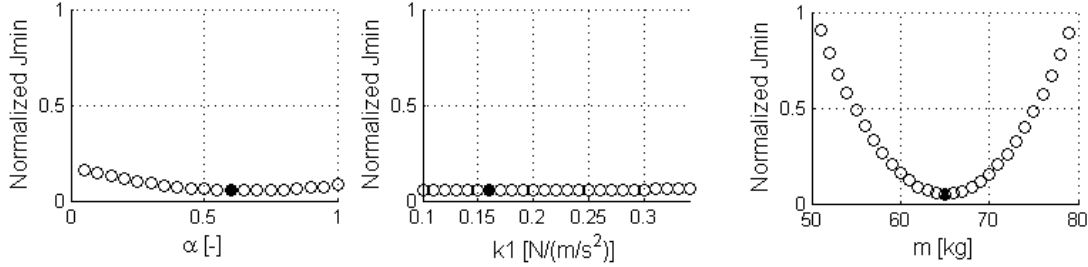
Figure 8: Plots of $J_{\min}$ versus a single parameter value, mass distribution α, air friction coefficient k_1 and total mass of the skater m, as the parameter is varied about the nominal value for rider 1 from Table 1. The filled circles corresponds to the value of $J_{\min}$ at the nominal parameter value.

5.3 Fitting false data

If the fits which are obtained are a result of good curve fitting, then it should be able to obtain good fits to false data. To test the model a pure sine function, $A \cos(2\pi t/T)$, , with amplitude A, and stroke time T, is added to the measured velocity data of the upper body in either directions. In Figure 9 the minimal error function versus the amplitude of the sinus wave is plotted. The total error between the model and the measured variables is minimal if the amplitude of the added function is zero. The model shows the best fit if there is not added corrupted data to the velocity data of the upper body. These results shows that the fits are not a result of good curve fitting, but rather the result of a good model.
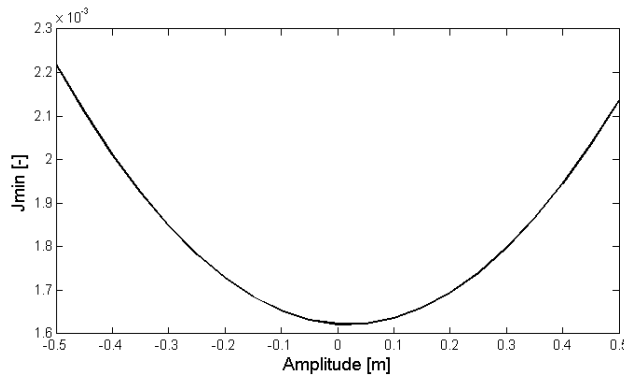
Figure 9: Plot of error $J_{\min}$ versus the amplitude of the sine wave corrupting the velocity data of the upper body of the skater

5.4 Kinematic complexity

The double stance phase was not included in the model. However, the sum of the measured left and right force during the double stance phase do correspond well with the calculated forces, which demonstrates that there is little need for modeling this short double stance phase.

13

Another major simplification of the model is that it was assumed that the center of mass remains at a constant height during skating, which was based on the Boer [3]. However, in accelerometer data of the upper body it was found that at the end of the stroke the upper body accelerates about 1.5 times gravity, which really influences the forces in the model. Therefore it seems beneficial to include the vertical motion of the body in the model.

6 CONCLUSIONS

We have constructed a simple 2-dimensional model of speed skating that does a reasonable job of imitating the forces and kinematics as observed in actual speed skating. The model reproduces these forces and motions reasonably well, even if we do not fit for that. The model is limited in accuracy due to the limited accuracy of the LPM position measurement system. Adding the (small) vertical motion of the upper body can increase the accuracy of the model.

The model seems promising for individual training advice. Coordination patterns of individual skaters can be optimized by using the model if psychological constraints of individual skater are added to the model. In Appendix F a detailed description of the needed constraints on the model is given. The model can also be used to give insight in the biomechanics of speed skating, like why speed skaters steer back to their body at the end of the stroke. Finally the effect of anthropometric differences between speed skaters can be determined.

APPENDIX

A Kinematic transformation

The differential algebraic (constraint) equations of motion (DAE's), without the non-holonomic skate constraint, from (11) can be written as,

$$\begin{bmatrix} \mathbf{M} & \mathbf{C}^T \\ \mathbf{C} & \emptyset \end{bmatrix} \begin{bmatrix} \ddot{\mathbf{x}} \\ \boldsymbol{\lambda} \end{bmatrix} = \begin{bmatrix} \mathbf{f} \\ \mathbf{hc} \end{bmatrix}, \tag{17}$$

with the COM accelerations $\ddot{\mathbf{x}}$, the diagonal mass matrix $\mathbf{M}$, the applied forces $\mathbf{f}$ at the COM, the Jacobian $\mathbf{C} = \partial \mathbf{c}/\partial \mathbf{x}$ of the constraint equations $\mathbf{c}(\mathbf{x}) = 0$, the convective terms $\mathbf{hc} = (\partial(\mathbf{C}\dot{\mathbf{x}})/\partial \mathbf{x})\dot{\mathbf{x}}$, and the Langrange multipliers $\boldsymbol{\lambda}$ (with respect to the constraints $\mathbf{c}$). The constrained equations of motion are,

$$\mathbf{M}\ddot{\mathbf{x}} = \mathbf{f} - \mathbf{C}^T \boldsymbol{\lambda}. \tag{18}$$

Next, we like to rewrite the equations in terms of the generalized coordinates $\mathbf{q}$. Therefore we introduce the coordinates of the COM $\mathbf{x}$ expressed in terms of the generalized coordinates $\mathbf{q}$,

$$\mathbf{x} = \mathbf{T}(\mathbf{q}) \tag{19}$$

Differentiate this twice with respect to time,

$$\dot{\mathbf{x}} = \mathbf{T}_{,\mathbf{q}}\dot{\mathbf{q}} \qquad \text{and} \qquad \ddot{\mathbf{x}} = \mathbf{T}_{,\mathbf{q}}\ddot{\mathbf{q}} + \mathbf{h} \tag{20}$$

The subscript comma followed by one or more variables denotes the partial derivatives with respect to these variables, and with the convective terms $\mathbf{h} = (\mathbf{T}_{,\mathbf{q}}\dot{\mathbf{q}})_{,\mathbf{q}}\dot{\mathbf{q}}$. Substitution of these accelerations in (18) and pre-multiplying with the transposed Jacobian $\mathbf{T}_{,\mathbf{q}}^T$ gives,

$$\mathbf{T}_{,\mathbf{q}}^T \mathbf{M}(\mathbf{T}_{,\mathbf{q}}\ddot{\mathbf{q}} + \mathbf{h}) = \mathbf{T}_{,\mathbf{q}}^T(\mathbf{f} - \mathbf{C}^T \boldsymbol{\lambda}) \tag{21}$$

Since the generalized coordinates fulfill the constraints, $\mathbf{T}_{,\mathbf{q}}^T \mathbf{C}^T$ is identical to zero, that is the constraint forces $\boldsymbol{\lambda}$ fall out of the equations. The result is the equations of motion expressed in terms of the generalized generalized coordinates $\mathbf{q}$,

$$\mathbf{T}_{,\mathbf{q}}\mathbf{M}\mathbf{T}_{,\mathbf{q}}^T \ddot{\mathbf{q}} = \mathbf{T}_{,\mathbf{q}}^T(\mathbf{f} - \mathbf{M}\mathbf{h}) \tag{22}$$

Finally the skate constraint can be added to these equations of motion, which results in the constraint equations of motion (14) and (15) .

B   State projection

After numerical integration of the equations of motion for one time increment, the state variables in general do not fulfill the constraints. This can be solved by formulating a minimization problem such that the distance from the predicted solution $\tilde{\mathbf{q}}_{n+1}$ to the solution which is on the constraint surface is minimal: $\|\tilde{\mathbf{q}}_{n+1} - \mathbf{q}_{n+1}\|_2 = \min_{\mathbf{q}_{n+1}}$ and where all $\mathbf{q}_{n+1}$ have to fulfill the constraints $\mathbf{c}(\mathbf{q}_{n+1}) = 0$. This non-linear constraint least-square problem is solved with a Gauss-Newton method after every numerical integration step.

C   Objective function $J_{\min}$

The best agreement between simulation and measurements can be achieved if we use accurate values for the air friction coefficient and the mass distribution. This is solved by minimizing the error between the model and the measurements. The objective function is defined by equation:

$$E_j = \frac{1}{N} \sum_{i=1}^{N} (\tilde{y}_i - y_i)^2 \tag{23}$$

where N the number of collected data points, y_i the measured value of the variable and $\tilde{y}_i$ the simulated value of the variable from the model. This is a constrained multi variable minimization problem: $\min_x f(x)$ with the constraint: $\mathrm{lb} \leq \mathrm{x} \leq \mathrm{ub}$ in which x are the air friction coefficient k_1 and mass distribution constant α. The upper and lower limit of α are defined as 0 and 1 while the limits of k_1 are defined as 0.1 and 0.3. With the optimization function *fmincon* of Matlab the optimal combination of α and k_1 are found. The optimization function uses an interior point algorithm and starts at the initial guess of the minimum x0. For each measured variable the optimal mechanical parameters can be fit.

Besides calculating the optimal values by minimizing one variable, the net error is calculated including the error of the upper body position, velocities and local normal forces (N_i). The net error is calculated with:

$$J_{\min} = \frac{\sum_{j=1}^{M} w_j \left(\frac{1}{N} \sum_{i=1}^{N} \frac{(\tilde{y}_{ij} - y_{ij})^2}{\bar{y}_j^2} \right)}{\sum_{j=1}^{M} w_j \bar{y}_j^2} \tag{24}$$

in which $\tilde{y}_{ij}$ is the simulated value of a variable, y_{ij} the measured value of a variable, w_j is the weighting factor of a variable and $\bar{y}_j$ is the characteristic value of the variable. The peak to peak values of the x and y upper body positions, average value of the body velocity in forward direction, peak to peak value of the velocity in sideward direction and the local measured normal peak force as the characteristic values of the parameters. Equal weights are used ($w_j = 1$) for all j in the error function.

D Synchronization method

The LPM position measurement system and the DAQ data acquisition unit are synchronized with video frames from a high speed camera (300 Hz).

D.1 Synchronization LPM and video

The LPM is synchronized by using an extra static transponder, which was placed in line with the start line on the ice. During the synchronization test the line is filmed with a high speed camera (300 Hz). The moment of crossing the start line can be found in the LPM data and video.

D.2 DAQ and video

In order to synchronize the DAQ and video frames a reset button with LED, which lights up when pressed, is used. The reset button is connected with the DAQ. At the start and the end of the measurement the subject has to push the reset button in view of the high speed camera, such that the video frames at which the LED reset button when pushed lights up can be easily determined.

E Friction estimation

In order to estimate the friction coefficients, the subjects got the following instruction: after skating two laps immediately stop skating and glide along the line of the lanes in the same skating posture as you were skating before for 100 m.
In order to determine the coefficients of friction from the glide exercise, it is assumed that the friction coefficients are constant during the glide.

From this estimation the conclusion is drawn that the speed should decreases linearly. A first order polynomial is fitted through the velocity profile of the LPM data of the COM of the skater during gliding.

$$\dot{y}(t) = -at + b \tag{25}$$

The gradient a of the line is the decelerations of the skater during gliding. The total friction force F_{friction} is the total mass m times the deceleration a of the skater during gliding; $F_{\text{friction}} = ma$. The air friction coefficient is assumed to behave like,

$$F_{\text{air}} = k_1 v^2 = \beta F_{\text{friction}}, \tag{26}$$

with the velocity v of the center of mass of the skater, k_1 the air drag factor and β the friction distribution factor which is assumed to be 0.8. The ice friction is assumed to behave like Coulomb friction as in

$$F_{\text{ice}} = \mu mg = (1 - \beta) F_{\text{friction}}, \tag{27}$$

where μ is the Coulomb friction coefficient between the ice and the skate.

F Optimization

Additional constraints are required to use the model for finding coordination patterns which results in optimal performance. The model has to be constrained by the physiology of the skater during optimization of his coordination pattern. The physiology constrains of a skater are given by: the leg length, average power and maximal power of the speed skater.

F.1 Leg length constraint

The leg length has to be constrained to be within the physiological limits of the skater.

F.2 Maximal power constraint

The maximal power during a single stroke must not exceed the maximal possible power from a leg extension motion of a skater. The maximal power constraint value could be based on either literature or experimentally determined. First, the maximal power can be determined from the push-off force and velocity of leg extension in the horizontal plane, since no work is done in the vertical plane. The maximal possible power of single leg extension as a function of the leg extension velocity can be based on force-velocity data extracted from leg press results of Vandervoort et al. [12]. The power is estimated by multiplying the force with the extension velocity of the leg [1] (Fig. 10).
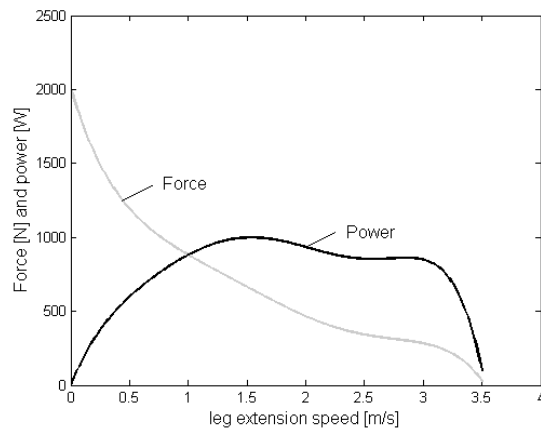
Figure 10: Force velocity relation [1]

Secondly, the maximal power of a single leg extension could be experimentally determined per subject. In power models the maximal and average power of an athlete is measured with an ergometer test [7]. The measured power is multiplied by a constant to find the power during skating. Recently, a new power measurement method is developed by O. den Braver. A speed skater has to make crossovers on a treadmill running at a constant speed. The speed skater has a band around his waist which is horizontal connected to the wall. With a force measurement device the forces in the band are measured. Finally the power is calculated by multiplying the measured forces with the speed of the treadmill.

F.3 Average power constraint

The average power of a stroke must not exceed the available aerobic power of a leg extension motion. The average power of a stroke can be calculated by:

$$P_{\text{avg}} = \frac{1}{t_{\text{stroke}}} \int_0^{t_{\text{stroke}}} P dt \tag{28}$$

In which t_{stroke} is the stroke time and P is the available aerobic power for skating. For this equation it is assumed that the skater is steady state speed, which results in zero anaerobic power.

The average power exerted during skating can be either measured with oxygen measurements during the speed skating measurements or calculated by Equation 28.

G Leg power calculation

For optimization the power exerted by the skater of stroke has to fulfill the constraints. The power of a stroke can be determined from the push-off force of the skate on the ice and the leg extension in the horizontal plane, since no work is done in the vertical plane (Eq. 29).

$$P_{leg} = F_{Tls} \dot{v}_{LS} \tag{29}$$

An example of the leg power during a stroke can be seen in Figure 11. At the beginning of the stroke the leg power becomes negative, which is caused by the negative direction of the lean angle. During the stroke the leg power increases to approximately 500 W. At the end of the stroke the extension speed decreases and the leg power becomes smaller.
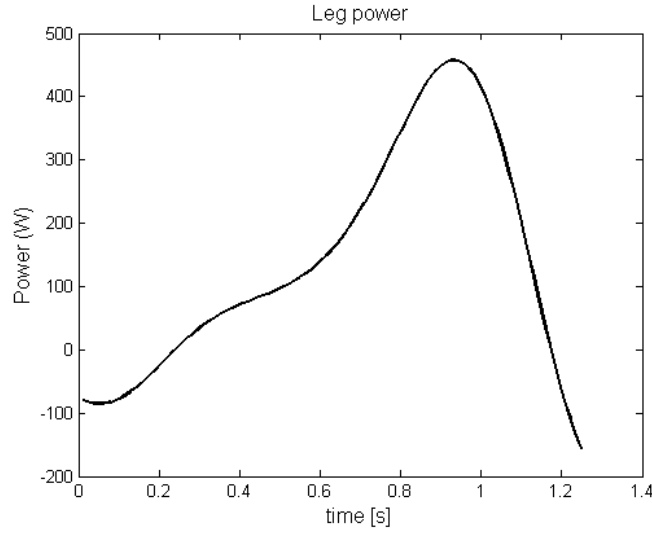
Figure 11: Leg power in horizontal plane

H Generalized coordinates

The positions of the bodies (B,LS,RS) written in the generalized coordinates:

$$
\begin{bmatrix}
x_B \\
y_B \\
x_{LS} \\
y_{LS} \\
x_{RS} \\
y_{RS}
\end{bmatrix}
=
\begin{bmatrix}
x_B \\
y_B \\
x_B - \cos(\theta_{LS}) u_{LS} - \sin(\theta_{LS}) v_{LS} \\
y_B + \sin(\theta_{LS}) u_{LS} - \cos(\theta_{LS}) v_{LS} \\
x_B - \cos(\theta_{RS}) u_{RS} - \sin(\theta_{RS}) v_{RS} \\
y_B - \sin(\theta_{RS}) u_{RS} + \cos(\theta_{RS}) v_{RS}
\end{bmatrix}
\tag{30}
$$

in which θ_i are the steer angles. These planar angular rotations can be calculated, since the velocity data of the skate in plane (x,y) are obtained. The steer angles are calculated by:

$$
\begin{bmatrix}
\theta_{LS} \\
\theta_{RS}
\end{bmatrix}
=
\begin{bmatrix}
-\tan^{-1}\left(\frac{\dot{y}_{LS}}{\dot{x}_{LS}}\right) \\
\tan^{-1}\left(\frac{\dot{y}_{RS}}{\dot{x}_{RS}}\right)
\end{bmatrix}
\tag{31}
$$

I Convective acceleration terms

The convective acceleration terms of the leg extension constraints are:

$$
\begin{aligned}
hc_1 ={}& \ddot{\theta}_{\text{LS}}(v_{\text{LS}}\cos(\theta_{LS}) - u_{\text{LS}}\sin(\theta_{LS})) + \ddot{u}_{\text{LS}}\cos(\theta_{LS}) + \ddot{v}_{\text{LS}}\sin(\theta_{LS}) - \\
& \dot{\theta}_{LS}(\dot{\theta}_{LS}(u_{\text{LS}}\cos(\theta_{LS}) + v_{\text{LS}}\sin(\theta_{LS})) - \dot{v}_{\text{LS}}\cos(\theta_{LS}) + \dot{u}_{\text{LS}}\sin(\theta_{LS})) + \\
& \dot{\theta}_{LS}\dot{v}_{\text{LS}}\cos(\theta_{LS}) - \dot{\theta}_{LS}\dot{u}_{\text{LS}}\sin(\theta_{LS})
\end{aligned}
\tag{32}
$$

$$
\begin{aligned}
hc_2 ={}& \ddot{v}_{\text{LS}}\cos(\theta_{LS}) - \ddot{\theta}_{LS}(u_{\text{ls}}\cos(\theta_{LS}) + v_{\text{LS}}\sin(\theta_{LS})) - \ddot{u}_{\text{LS}}\sin(\theta_{LS}) - \\
& \dot{\theta}_{LS}(\dot{\theta}_{LS}(v_{\text{LS}}\cos(\theta_{LS}) - u_{\text{LS}}\sin(\theta_{LS})) + \dot{u}_{\text{LS}}\cos(\theta_{LS}) + \dot{v}_{\text{LS}}\sin(\theta_{LS})) - \\
& \dot{\theta}_{LS}\dot{u}_{\text{LS}}\cos(\theta_{LS}) - \dot{\theta}_{LS}\dot{v}_{\text{LS}}\sin(\theta_{LS})
\end{aligned}
\tag{33}
$$

$$
\begin{aligned}
hc_3 ={}& \ddot{u}_{\text{RS}}\cos(\theta_{RS}) - \ddot{\theta}_{RS}(-v_{\text{RS}}\cos(\theta_{RS}) + u_{\text{RS}}\sin(\theta_{RS})) + \ddot{v}_{\text{RS}}\sin(\theta_{RS}) - \\
& \dot{\theta}_{RS}(\dot{\theta}_{RS}(u_{\text{RS}}\cos(\theta_{RS}) + v_{\text{RS}}\sin(\theta_{RS})) - \dot{v}_{\text{RS}}\cos(\theta_{RS}) + \dot{u}_{\text{RS}}\sin(\theta_{RS})) - \\
& \dot{\theta}_{RS}\dot{-v}_{\text{RS}}\cos(\theta_{RS}) - \dot{\theta}_{RS}\dot{u}_{\text{RS}}\sin(\theta_{RS})
\end{aligned}
\tag{34}
$$

$$
\begin{aligned}
hc_4 ={}& \dot{\theta}_{RS}(\dot{\theta}_{RS}(-v_{\text{RS}}\cos(\theta_{RS}) + u_{\text{RS}}\sin(\theta_{RS})) - \dot{u}_{\text{RS}}\cos(\theta_{RS}) + \dot{v}_{\text{RS}}\sin(\theta_{RS})) + \\
& \ddot{v}_{\text{RS}}\cos(\theta_{RS}) - \ddot{u}_{\text{RS}}\sin(\theta_{RS}) - \ddot{\theta}_{RS}(u_{\text{RS}}\cos(\theta_{RS}) + v_{\text{RS}}\sin(\theta_{RS})) - \\
& \dot{\theta}_{RS}\dot{u}_{\text{RS}}\cos(\theta_{RS}) - \dot{\theta}_{RS}\dot{v}_{\text{RS}}\sin(\theta_{RS})
\end{aligned}
\tag{35}
$$

The convective acceleration terms of the skate constraints are:

$$
\begin{aligned}
hc_5 ={}& \dot{\theta}_{LS}\dot{u}_{\text{LS}} - \ddot{v}_{\text{LS}} + \ddot{\theta}_{LS}u_{\text{LS}} + \dot{\theta}_{LS}\dot{x}_B\cos(\theta_{LS}) - \dot{\theta}_{LS}\dot{y}_B\sin(\theta_{LS}) \\
hc_6 ={}& \dot{\theta}_{RS}\dot{u}_{\text{RS}} - \ddot{v}_{\text{RS}} + \ddot{\theta}_{RS}u_{\text{RS}} + \dot{\theta}_{RS}\dot{x}_B\cos(\theta_{RS}) + \dot{\theta}_{RS}\dot{y}_B\sin(\theta_{RS})
\end{aligned}
\tag{36}
$$

REFERENCES

[1] Allinger, T.L., Bogert, A.J. vd, *Skating technique for the straights, based on the optimization of a simulation model*, Medicine & Science in Sports & Exercise **29**(2), 279-286, 1997

[2] Boer, R.W. de, Schermerhorn P., Gademan, J., Groot G., de, and Ingen Schenau, G.J. van, *Characteristic Stroke Mechanics of Elite and Trained Male Speed Skaters*, Int. J. Sport. Biomech. **2**, 175-185, 1986

[3] Boer, R.W. de, Nislen, K.L., *The gliding and push-off technique of male and female Olympic speed skaters*, Int. J. Sport. Biomech. **5**, 119-134, 1989

[4] Cabrera, D., Ruina, A., Kleshnev, V., *A simple 1+ dimensional model of rowing mimics observed forces and motions*, Human Movement Science **25**, 192-220, 2006

[5] Fintelman, D.M., *Literature study: Biomechanical models for speed skating*, Technical University Delft, 2010

[6] Ingen Schenau, G.J. van, *The influence of air friction in speed skating*, J. Biomechanics, 15(6), 449-458

[7] Koning, J.J. de, Ingen Schenau, G.J. van, *Performance-determining factors in speed skating*, editor:Vladimir Zatsiorsky, Biomechanics in sport: Performance enhancement and injury prevention: Olympic Encyclopadia of sports medicine, Volume IX, ISBN 978-0-632-05392-6, 2000

[8] Koning, J.J. de, *Biomechanical aspects of speed skating*, Academic thesis of the Free University of Amsterdam, ISBN 90-9003956-2, 1991

[9] Koning, J.J. de, Groot, G. de, Ingen Schenau, G.J. van, *Ice friction during speed skating*, J. Biomechanics, **25**(6), 565-571, 1992

[10] McLean, S.G., Su, A., Van den Bogert, A.J., *Development and validation of a 3-D model to predict knee joint loading during dynamic movement*, Journal of Biomechanical Engineering, **125**, 864-874, 2003

[11] Otten, E., *Inverse and forward dynamics: models of multi-body systems*, Phil. Trans. R. Soc. Lond., **358**, 1493-1500, 2003

[12] Vandervoort, A.A.; Sale, D.G.; and Moroz J. *Comparison of motor unit activation during unilateral and bilateral leg extension*, J. Sport. Sci., **13**, 153-170, 1995